

# Reversal of Clar's Aromatic-Sextet Rule in Ultrashort Single-End-Capped [5,5] Carbon Nanotubes

Guglielmo Monaco,<sup>[a]</sup> Emeritus Lawrence T. Scott,<sup>[b]</sup> and Riccardo Zanasi\*<sup>[a]</sup>

The three-fold HOMO-LUMO gap oscillation, typical of finite length armchair carbon nanotubes (CNT), has a major effect on the magnetic response of ultrashort, single-end-capped [5,5] carbon nanotubes to a perturbing magnetic field parallel to the main symmetry axis. For the CNT's containing 40, 70, and 100 carbon atoms, for which 100% of the C=C double bonds can be grouped into aromatic-sextets, i.e., fully or complete Clar networks, large paratropic (antiaromatic) global circulations around the cylindrical axis are predicted at the DFT level of calculation. Local and semi-global diatropic (aromatic) currents

of strengths not larger than that of the benzene molecule are determined for a perpendicular perturbing magnetic field. CNTs of intermediate lengths do not display this enhanced antiaromatic response. The paratropic current flow clearly shows that these complete Clar networks can be viewed as stacked cycloparaphenylene belts, each providing a double  $4n$  annulene circuit as a consequence of the quinoidal resonance structure that results from their closure. Paradoxically, the fully aromatic Clar structure itself is responsible for the enhanced global antiaromaticity.

## 1. Introduction

The magnetic response of the ultrashort carbon nanotube  $C_{50}H_{10}$  a geodesic polyarene recently prepared by bottom-up chemical synthesis,<sup>[1]</sup> has been investigated. Interest on this compound rested on the possibility to use it as an end-capped template for growing a single-walled carbon nanotube (SW-CNT) of uniform diameter and single chirality, in this case an armchair [5,5]CNT. The growing process was devised to take place by means of Diels-Alder cycloaddition of ethyne molecules, or some synthetic equivalent, on the rim of the elongating CNT. Despite the many attempts developed so far, this kind of synthesis remains unaccomplished.<sup>[2–7]</sup>

To look for some specific reason which could prevent any further elongation of the  $C_{50}H_{10}$  ultrashort CNT, we have anticipated the calculation of the magnetically induced current density, and related properties, for the series  $C_nH_{10}$ ,  $n = 40, 50, \dots, 100$  displayed in Figure 1, looking for a connection between the aromatic/antiaromatic character of these species and the peculiar three-fold oscillation behavior, already

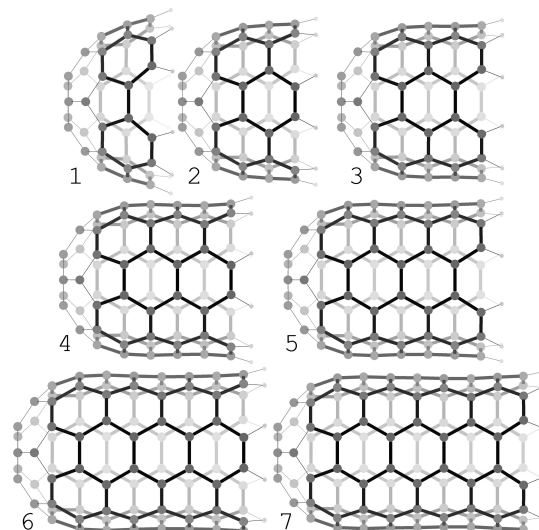


**Figure 1.** Ultrashort [5,5] SW-CNT considered in the present study: top row:  $C_{40}H_{10}$  (1),  $C_{50}H_{10}$  (2),  $C_{60}H_{10}$  (3); middle row:  $C_{70}H_{10}$  (4),  $C_{80}H_{10}$  (5); bottom row:  $C_{90}H_{10}$  (6),  $C_{100}H_{10}$  (7). Benzene rings in bold, end-caps in light.

very well known from previous studies, concerning HOMO-LUMO gaps, activation energies, standard enthalpy of formations and NICS values, see hereafter for details. In general, for one-end capped arm-chair  $[p,p]$ CNT's, the oscillation of the above mentioned properties occurs every three additions of  $2p$  carbon atoms to form a new terminal  $[4p]$ annulene after each addition. To the best of our knowledge, previous recognition of similar ternary oscillations were reported for the HOMO-LUMO gap<sup>[8–14]</sup> of open, one-end closed, or two-ends closed armchair CNT's,<sup>[11,12,14]</sup> for the activation energy of the Diels-Alder cycloaddition of a single ethyne molecule for the growing process of an arm-chair CNT,<sup>[4]</sup> for the standard enthalpy of formation of [5,5]CNT of different finite lengths [12] and for the NICS evaluated in the ring center of CNT.<sup>[13,15,16]</sup> Even for long [6,6]

[a] Dr. G. Monaco, Prof. R. Zanasi  
Dipartimento di Chimica e Biologia "A. Zambelli"  
Università degli studi di Salerno  
via Giovanni Paolo II 132  
Fisciano 84084, SA (Italy)  
E-mail: rzanasi@unisa.it  
gmonaco@unisa.it

[b] Prof. E. L. T. Scott  
Department of Chemistry  
University of Nevada  
Reno, NV 89557-0216 (USA)  
E-mail: lawrence.scott@BC.edu

Supporting information for this article is available on the WWW under <https://doi.org/10.1002/open.202000091>

© 2020 The Authors. Published by Wiley-VCH Verlag GmbH & Co. KGaA. This is an open access article under the terms of the Creative Commons Attribution Non-Commercial NoDerivs License, which permits use and distribution in any medium, provided the original work is properly cited, the use is non-commercial and no modifications or adaptations are made.

CNT fragments, a Clar-Kekulé oscillations has been reported analyzing bond lengths distribution.<sup>[17]</sup>

## 2. Result and Discussion

Many well accepted methods for the detection and quantification of the aromatic and/or antiaromatic character of a molecule are based on the magnetic criterion, which ultimately requires the calculation of the magnetically induced current density. Current density maps alone provide only a semi-quantitative indication on the magnetically induced electron flow. Nonetheless, this often suffices to establish if a compound is aromatic, antiaromatic or nonaromatic.<sup>[18]</sup> However, a fully quantitative magnetic indicator of aromaticity/antiaromaticity can be obtained calculating the so called current strength, or current susceptibility,<sup>[19,20]</sup> which turns out to be a rather convenient choice since, unlike NICS<sup>[21,22]</sup> or other quite popular magnetic indicators of aromaticity, it does not depend explicitly on any geometrical parameter.<sup>[23,24]</sup> It should be noted that, although present computational methods allow the direct computation of currents, the NICS-XY scan, which is a non-quantitative indirect method, has also been found capable of a correct inference of the tropicities in many polycyclic systems.<sup>[25–27]</sup>

Curved molecules represent a challenge for the production of meaningful current density maps and some special strategy must be adopted to work them out. Corannulene, with its bowl-shaped geometry, was one of the first studied molecules of this type. In that case current density maps were reported using an exploded view where the current vectors are projected in a plane parallel to the individual ring, at a distance of  $1a_0$  from it inside and outside the bowl.<sup>[28]</sup> A different approach was used to produce 3D current density maps for Buckminsterfullerene, in which the magnetically induced current density was obtained at selected points in space.<sup>[29]</sup> The SOP (stack of plates) method was also proposed to visualize aromaticity of bowl-shaped molecules.<sup>[30]</sup> Current density maps here in the following and collected within the Supplementary Information have been obtained using our own approach, which was developed for visualizing the induced current density in charged corannulene species.<sup>[31]</sup> Accordingly, current density vectors are plotted on a pair of surfaces having the molecular shape at  $0.8 \text{ \AA}$  inside and outside the ultrashort carbon nanotubes. To the best of our knowledge, a previous investigation of ring currents in carbon nanotubes has been presented by Ren and coworkers in Ref. [32].

A first estimate of the induced current magnitude can be grasped considering the size of the plotted arrows, see Figure 2 in the case of  $C_{50}H_{10}$  for a perturbing magnetic field parallel to the main symmetry axis, especially in comparison with those in maps of reference molecules, as, for example, the benzene or corannulene current density maps shown in the Supporting Information (see Figures S2 and S4). Even at this stage, it is quite evident as the current density strength, for an inducing magnetic field parallel to the main symmetry axis of the molecules, is very amplified in the case of the  $C_{70}H_{10}$  and

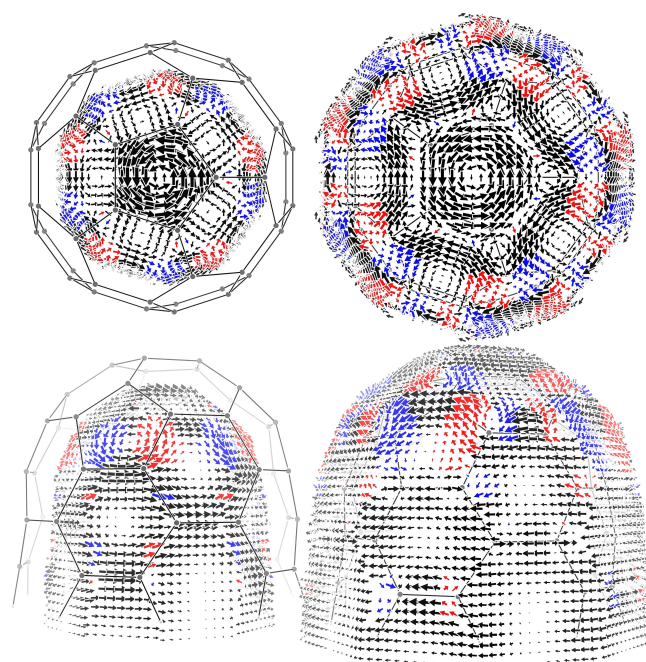


**Figure 2.** Current density field induced in the electron cloud of  $C_{50}H_{10}$  by a unitary magnetic field  $B = k$  parallel to the main symmetry axis of the molecule. Vectors are plotted on a surface having the tubular shape at  $0.8 \text{ \AA}$  inside on the left and outside on the right of the figure. First row shows a top view, second row shows a side view. Red/blue color indicates that parallel/antiparallel vector component is 30% of the vector modulus at least.

$C_{100}H_{10}$ , molecules both inside and outside the tubes, see Figures S12 and S13, where the current is circulating in the paratropic sense. For  $C_{50}H_{10}$ ,  $C_{60}H_{10}$ ,  $C_{80}H_{10}$ , and  $C_{90}H_{10}$  the parallel perturbation does not provide such a strong induced current, which is, however, mainly paratropic only inside the tubes and predominantly diatropic on the outside, see Figures 2, S12, and S13. Thus, a three-fold oscillating response to the parallel perturbation can be readily noticed, which is neatly paratropic (antiaromatic) in the response spikes. For a magnetic field perpendicular to the main symmetry axis, the induced current does not show such an oscillating behavior, see Figures S9, S10, S14, and S15. Therefore, it seems quite clear that the three-fold current fluctuation is a feature only of the parallel response to the magnetic perturbation, which can be discussed in terms of frontier orbital symmetries, as given in the following.

Aside this qualitative picture, which can only be partially informative, a more accurate and quantitative view can be obtained using net bond current strengths,<sup>[19,20,33]</sup> which have been calculated for all C=C bonds of the systems here studied and shown in Figures 3 and 4 for an inducing magnetic field parallel and perpendicular, respectively, to the main symmetry axis of the molecules, see the Supplementary Information for computational details.

In both the figures, net current strengths are represented as an arrow on the corresponding C=C bond showing the resultant direction of the integrated current density; beside each arrow a figure indicates the net current strength value in

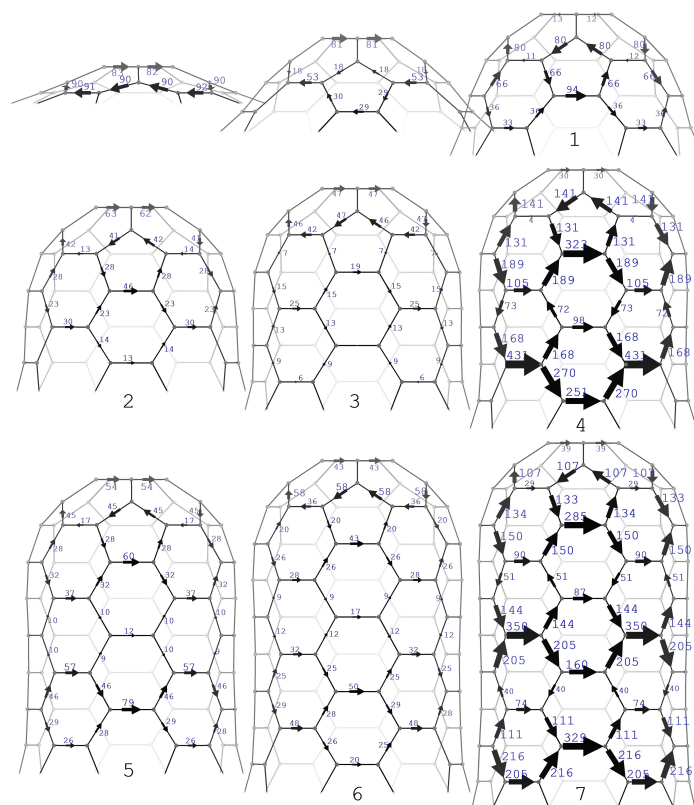


**Figure 3.** Net C=C bond current strengths calculated for a magnetic field parallel to the main symmetry axis and pointing from bottom to top. Values aside each arrow represent the percentage relationship with respect to the diatropic benzene current strength of 12 nA/T. Circulation from left to right are globally paratropic/antiaromatic. Corannulene and  $C_{30}H_{10}$  are also reported, first two molecules in the first row.

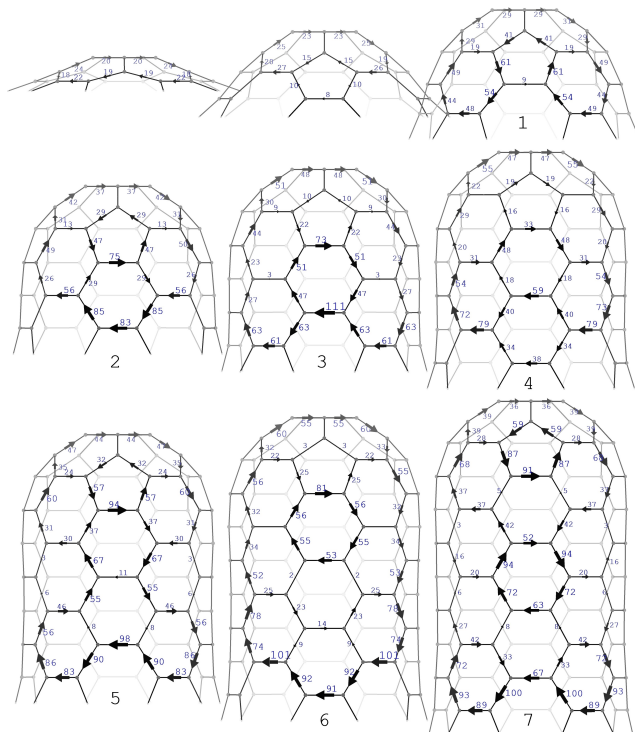


**Figure 4.** Net C=C bond current strengths calculated for a magnetic field perpendicular to the main symmetry axis and pointing toward the observer. Diatropic/paratropic circulations are clockwise/anticlockwise. See Figure 3 for further details.

percentage relationship with respect to the standard value of 12.0 nA/T of the benzene net (diatropic) current strength, calculated at the same level of basis set and density functional, see Table S3. For the sake of the discussion, both figures report also net current strengths calculated for the corannulene and  $C_{30}H_{10}$  molecules.

As an example of the adopted procedure, we consider the net current strengths calculated for the “horizontal” C=C bonds of  $C_{50}H_{10}$ , reported in Table S6 for a perturbing magnetic field parallel to the main symmetry axis and obtained integrating the cross section of the current density included in the domains shown in Figure S8. These net current strengths are 7.5, −1.6, 5.5, 3.6, and 1.6 nA/T going down from the top pentagonal ring of the corannulene fragment toward the open end side (positive/negative values indicate paratropic/diatropic sense). Taking the absolute value they correspond to 63%, 13%, 46%, 30%, and 13% (see Figure 3) of the reference benzene current strength. The same procedure has been adopted to report all the calculated current strengths, comprising also those resulting from the perpendicular perturbation, see, for example, Table S7 and Figure S11 for current strengths and integration domains in the case of a perturbing magnetic field perpendicular to the main symmetry axis of  $C_{50}H_{10}$ .

Despite the absence of a symmetry plane perpendicular to the principal axis, and thus with the loss of a strict symmetry classification of the molecular orbitals as  $\sigma$  and  $\pi$ , orbitals can

**Table 1.** HOMO, LUMO, HOMO→LUMO, and HOMO→LUMO + 1 symmetries.

CNT	HOMO-1	HOMO	LUMO	LUMO + 1	HOMO→LUMO	HOMO→LUMO + 1
C <sub>20</sub> H <sub>10</sub>	E <sub>1</sub>	E <sub>1</sub>	E <sub>1</sub>	E <sub>1</sub>	A <sub>1</sub> ⊕ [A <sub>2</sub> ] ⊕ E <sub>2</sub>	=
C <sub>30</sub> H <sub>10</sub>	E <sub>1</sub>	E <sub>1</sub>	E <sub>1</sub>	E <sub>1</sub>	A <sub>1</sub> ⊕ [A <sub>2</sub> ] ⊕ E <sub>2</sub>	=
C <sub>40</sub> H <sub>10</sub>	E <sub>2</sub>	A <sub>2</sub>	A <sub>1</sub>	E <sub>1</sub>	A <sub>2</sub>	E <sub>1</sub>
C <sub>50</sub> H <sub>10</sub>	E <sub>1</sub>	A <sub>2</sub>	E <sub>1</sub>	A <sub>1</sub>	E <sub>1</sub>	A <sub>2</sub>
C <sub>60</sub> H <sub>10</sub>	A <sub>2</sub>	A <sub>1</sub>	A <sub>2</sub>	E <sub>1</sub>	A <sub>2</sub>	E <sub>1</sub>
C <sub>70</sub> H <sub>10</sub>	A <sub>2</sub>	A <sub>1</sub>	A <sub>2</sub>	E <sub>1</sub>	A <sub>2</sub>	E <sub>1</sub>
C <sub>80</sub> H <sub>10</sub>	A <sub>1</sub>	A <sub>2</sub>	A <sub>1</sub>	E <sub>1</sub>	A <sub>2</sub>	E <sub>1</sub>
C <sub>90</sub> H <sub>10</sub>	A <sub>2</sub>	A <sub>1</sub>	A <sub>2</sub>	E <sub>1</sub>	A <sub>2</sub>	E <sub>1</sub>
C <sub>100</sub> H <sub>10</sub>	A <sub>2</sub>	A <sub>2</sub>	A <sub>1</sub>	E <sub>1</sub>	A <sub>2</sub>	E <sub>1</sub>

still be labelled as *quasi-σ* and *quasi-π* according to a larger/smaller electron density at the atoms and at the middle of C=C bonds, and this labelling has been profitably used to understand the magnetic response in previous studies.<sup>[34,35]</sup> Noteworthy, since the current density induced in the  $\sigma$ -electrons in this kind of molecule, similarly to corannulene as well as in all sorts of planar aromatics hydrocarbons, is almost completely local to carbon atoms and C=C bonds,<sup>[33]</sup> it turns out that the net current strengths here reported are a reliable measure of  $\pi$ -aromaticity or  $\pi$ -antiaromaticity.

Looking at Figure 3, the three-fold current fluctuation characterizing the parallel response to the magnetic perturbation is very clear. In particular, C<sub>40</sub>H<sub>10</sub>, C<sub>70</sub>H<sub>10</sub> and C<sub>100</sub>H<sub>10</sub> show paratropic currents bandaging these ultrashort nanotubes with spikes of current as large as four times the reference benzene ring current. In this triad the current flow bifurcates and gathers around the six-membered rings of stacked cycloparaphenylene belts. These rings are those hosting a Clar's sextets in the corresponding nanobelts obtained removing the radialene cap to form a fully-Clar structure. Intermediate C<sub>50</sub>H<sub>10</sub>, C<sub>60</sub>H<sub>10</sub> and C<sub>80</sub>H<sub>10</sub>, C<sub>90</sub>H<sub>10</sub> ultrashort CNT's do not display such large current strengths, which remain, however, predominantly paratropic and lower in absolute value than the benzene reference current strength. In summary, when the magnetic field is applied parallel to the principal axis, local currents can be observed only in coincidence with the pentagonal rings forming the cap, otherwise currents are always distributed along a cycloparaphenylene belts. In other words, the antiaromaticity comes from the superaromaticity and not from individual paratropic currents. This is in contrast to the case of the field being perpendicular to the principal axis, discussed hereafter, where the ring currents are mostly localized within individual rings.

For the response to a magnetic field perpendicular to the main symmetry axis, see Figure 4, the periodic fluctuation of the current density is absent, as already observed looking at the current density maps. The general trend is that of diatropic (aromatic) circulations in contrast with the paratropic (antiaromatic) response to the parallel perturbation. As can be observed, C=C bond current strengths are in general lower than, and only in a few cases equal to, the benzene reference value. Currents local to six-member rings embedded within semi-global circulations are quite evident. Then, a dual behavior is found that seems a characteristic feature of this kind of species, comprising ultrashort CNT's and nanobelts.<sup>[36]</sup>

The exaltation of the current density for the parallel perturbation suggests a symmetry selection, which is magnified only in some cases by the frontier orbital gap.<sup>[37,38]</sup> To best appreciate that, we have collected in Table 1 the symmetries of the HOMO-1, HOMO, LUMO, and LUMO + 1 along with the symmetries of their products. As can be noticed, the product of the HOMO and LUMO symmetries provides, or it contains, with the only exception of C<sub>50</sub>H<sub>10</sub>, the irreducible representation A<sub>2</sub>, which matches exactly the symmetry of the rotation around the main symmetry z-axis. For C<sub>50</sub>H<sub>10</sub> the HOMO→LUMO + 1 virtual transition is of A<sub>2</sub> symmetry. This behavior is typical of antiaromatic species, for which a significant paratropic contribution to the current density can be predicted.<sup>[37,38]</sup> On the other hand, rotations around x and y are partners of the E<sub>1</sub> symmetry, then some paratropic contributions to the current density, induced by a perpendicular magnetic field arising from the HOMO→LUMO + 1 virtual transition can also be expected to occur.

The calculated three-fold oscillation of the HOMO-LUMO gap is reported in Figure 5. In agreement with previous reports,<sup>[8-14]</sup> the characteristic convergence of the HOMO and LUMO energies of the triad formed by the CNTs containing 40,

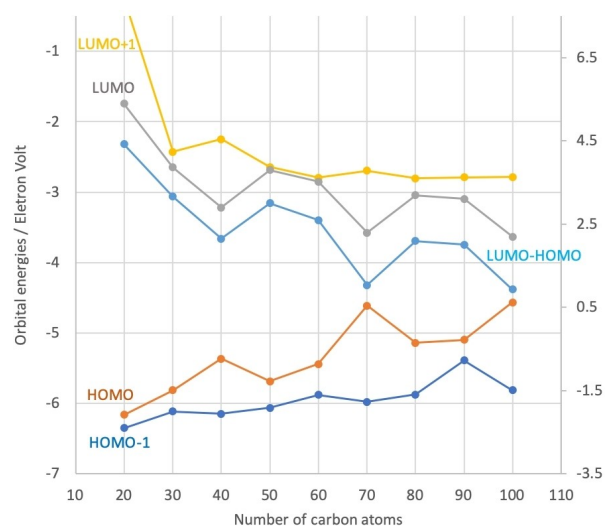


**Figure 5.** Calculated HOMO-1, HOMO, LUMO, and LUMO + 1 energies, to be read on the left vertical axis. The three-fold LUMO-HOMO gap oscillation, to be read on the right vertical axis, results from opposite oscillation of the HOMO and LUMO energies. HOMO-1 and LUMO + 1 do not show any marked energy oscillation.

70, and 100 carbon atoms can be readily observed. The combination of this exceptional reduction of the HOMO-LUMO gap with the symmetry of the corresponding virtual transition provides an immediate explanation of the peculiar magnetic response predicted for the parallel perturbation, in particular for  $C_{70}H_{10}$  and  $C_{100}H_{10}$  ultrashort one end capped [5,5] carbon nanotubes.

In addition to the magnetic response, the dual aromatic/antiaromatic character of the nanotubes can be accessed by energy. While addition of benzenoid rings to a graphene sheet can be generally expected to increase delocalization and stability, its wrapping to yield a tube can generate  $4n$  circuits which are associated with energy destabilization. The energy change due to these circuits is referred to as super(anti) aromaticity.<sup>[39,40]</sup> In addition to topological methods, a procedure to estimate this effect at the ab initio level has been investigated in a previous paper,<sup>[36]</sup> where fragments of increasing length of the tube have been considered to setup an homodesmotic reaction. In order to apply that procedure to the end-capped nanotubes, we have disregarded the radialene cap, considering that the trend of energy gaps and acetylene addition activation energies of tubes and end-capped tubes are parallel, but for a shift of 10 carbon atoms.<sup>[4]</sup> This procedure could be applied with some confidence to cap-less nanotubes  $C_{30}H_{20}$ ,  $C_{40}H_{20}$ ,  $C_{60}H_{20}$ ,  $C_{80}H_{20}$  (corresponding to capped-nanotubes  $C_{40}H_{10}$ ,  $C_{50}H_{10}$ ,  $C_{70}H_{10}$ ,  $C_{90}H_{10}$ ) yielding energy changes due to super-aromatization of roughly +1, +1, +4, -16 kcal mol<sup>-1</sup>, see Table S11 for the energy of nanotube fragments used to estimate the super-aromaticity stabilization. Notably, the largest destabilization is found for the  $C_{60}$  nanotube, with fixed Clar sextets.

That there is a connection between the three-fold periodicity and fully benzenoid CNTs, i.e., all  $\pi$ -electrons represented by aromatic Clar's sextets, is clear since their discovery and it is consistent with the necessary criterion for conductivity in CNTs, for which only fully benzenoid CNTs are metallic.<sup>[41,42]</sup> On the other hand, it is not yet clear why the complete Clar networks display small HOMO-LUMO gap, in contrast with that of planar polycyclic aromatic hydrocarbons in which the fully benzenoid structures are known to have large HOMO-LUMO gap.<sup>[8,13]</sup> Even the activation energy of the Diels-Alder cycloaddition runs counter<sup>[4]</sup> the longstanding aromatic-sextet rules of Eric Clar, rules that have proven so useful in successfully predicting the properties and reactivity of ordinary polycyclic aromatic hydrocarbons.<sup>[43,44]</sup>

The exception to the Clar aromatic-sextet rule finds an explanation in light of the dual antiaromatic/aromatic character featuring this kind of species, which cannot be recognized on the basis of the simple NICS analysis previously reported.<sup>[13,42]</sup> Once accepting that, the real question is why the antiaromatic character takes over for the fully benzenoid structures. The current density maps offer one possible explanation in terms of stacked cycloparaphenylene units. To see that, let us first consider one penta-*p*-phenylene chain, which is a fully benzenoid hydrocarbon having 2<sup>5</sup> resonance structures. Closing the penta-*p*-phenylene chain to form a [5]cycloparaphenylene belt increases the number of resonance structures by one, i.e., a

quinoidal structure where rings are connected by double bonds. This resonance structure provides two antiaromatic circuits formed by 20 carbon atoms each. The current induced by a magnetic field parallel to the central axis will be paratropic bifurcating and gathering around the Clar sextets and doubling its strength over the bonds connecting the rings. This picture is readily observed for  $C_{40}H_{10}$  in the top right corner of Figure 3.  $C_{70}H_{10}$  and  $C_{100}H_{10}$  are fully benzenoid systems which can be seen as two and three, respectively, stacked [5]cycloparaphenylene belts, as clearly evidenced by the bifurcating and gathering paratropic current around the Clar sextets, see right side of Figure 3. Intermediate CNTs do not have fixed Clar sextets, consequently the paratropic circuits around the tube are much less important.

Theoretical investigations have shown that Clar's theory should find limitations when going to large systems, that were not objects of consideration by Clar himself.<sup>[40,45,46]</sup> The present investigation adds a new warning to the applicability of Clar's theory. Indeed, Clar did not consider tubes or hollow molecules, where aromaticity acquires a new dimension coming from current circulating around the hole (super-aromaticity). The currents reported and the small gaps hint at an additional breakdown of the general correlation between thermodynamic and kinetic stability which holds in most benzenoid hydrocarbons<sup>[47,48]</sup> and is an implicit assumption of Clar theory.

## 2.1. Magnetic Properties

The magnetically induced current can be used to calculate first-order magnetic properties such as magnetizability ( $\xi_{\alpha\beta}$ ) and nuclear magnetic shielding constants,<sup>[49]</sup> which, in turn, display the threefold oscillation perhaps even more markedly. NMR Shielding constants can be converted in chemical shifts ( $\delta$ ) for easier comparison to experimental data, see Supporting Information.

Since experimental data are available for the NMR chemical shift of  $C_{50}H_{10}$ ,<sup>[1]</sup> it is worth making first a comparison with their predicted values in order to have a clear perception of the quality of the calculations. This is shown in Table 2, where equivalent carbon atoms have been enumerated from the pentagonal ring within the capped terminal to the open side of the molecule. As can be observed the matching with the experimental values is very good and permits a safe assignment of the various set of equivalent carbon atoms to the corresponding spectral line.

**Table 2.** C and <sup>1</sup>H NMR chemical shift (in ppm) respect to TMS for the  $C_{50}H_{10}$  ultrashort CNT.

Nucleus	GIAO	CTOCD-DZ2	Exp. <sup>[1]</sup>
C <sub>1</sub>	153.8	152.6	151.5
C <sub>6</sub>	155.8	154.8	154.1
C <sub>11</sub>	145.9	144.7	144.7
C <sub>21</sub>	138.5	137.4	137.6
C <sub>31</sub>	130.5	129.7	130.6
C <sub>41</sub>	125.5	125.4	126.4
H <sub>1</sub>	7.68	7.47	7.63

On this basis, we can look with confidence to the predicted magnetic properties and, in particular, to the oscillating behavior. A plot of the calculated components and average value of the magnetizability tensors versus the CNT length is shown in Figure 6, see also Table S8 for numerical details. Remarkably,  $\xi_{||} = \xi_{zz}$  turns out to be positive for the  $C_{70}H_{10}$  and  $C_{100}H_{10}$  molecules, which makes the two CNT's very low diamagnetic in average.

Employing a functional with a significantly larger percentage of HF exchange, like M06-2X having 54% HF exchange,<sup>[50]</sup> as recommended by some authors,<sup>[51–57]</sup> does not change the picture qualitatively. Although  $\xi_{||}$  turns out to be roughly halved using the M06-2X functional, it remains largely positive for both molecules, confirming the antiaromatic response for the parallel perturbation. The net paratropic current flowing over stacked cycloparaphenylene belts is confirmed at the M06-2X level as shown in Figure S15. The proton chemical shift calculated for  $C_{70}H_{10}$  and  $C_{100}H_{10}$  reaches the quite uncommon downfield values of 12.5 and 13.4 ppm (10.7 and 12.1 ppm at M06-2X level), respectively, see also Table S9 for further details.

These rather unusual results strongly suggest consideration of the stabilities of these molecules, which have been checked with respect to the lowest singlet and triplet excited states, adopting the same level of theory. As shown in Table S10 and Figure S16, the three-fold periodicity appears once again with minima for the  $C_{40}H_{10}$ ,  $C_{70}H_{10}$  and  $C_{100}H_{10}$  ultrashort CNT's. Although singlet instabilities have not been detected, the last two show a triplet instability.

### 3. Conclusions

The study of the magnetically induced current density in a series of ultrashort one-end capped [5,5] carbon nanotubes, starting from corannulene and adding a 10-carbon-atoms rim to the open-end tail up to  $C_{100}H_{10}$ , has permitted to generalize the double aromatic/antiaromatic character that features these species,<sup>[36]</sup> otherwise not permissible by using different techniques, though popular, as for example NICS.<sup>[21,22,13,42]</sup> Over a period of three additions the antiaromatic degree takes over the aromatic degree, providing the already well know three fold periodicity of the HOMO-LUMO gap, standard formation

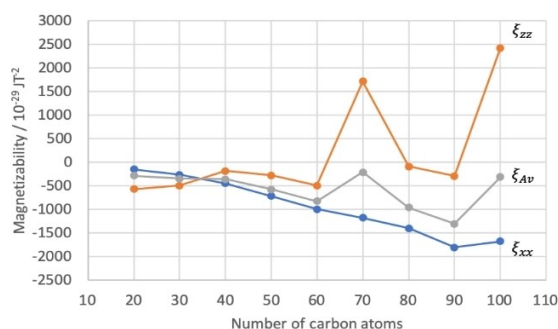


Figure 6. Calculated magnetizability tensor components versus CNT length.

enthalpy, and cycloaddition activation energy of a single ethyne molecule. In contrast with previous convictions, the enhanced antiaromaticity happens when a complete Clar network can be attributed to a CNT, since the Clar structure itself provides a stack of double  $4n$  annulenes as a consequence of the quinoidal resonance structure that results from the tube closure.

### Computational Methods

Equilibrium geometries have been calculated using the Gaussian'09<sup>[58]</sup> package at the B3LYP density functional theory<sup>[59]</sup> adopting the 6-31G(1d,1p)<sup>[60]</sup> basis set, under the  $C_{5v}$  symmetry point group constraint. In the case of  $C_{50}H_{10}$  an excellent agreement is found when comparing theoretical bond lengths with the available experimental data obtained from X-ray diffraction,<sup>[1]</sup> see Table S1 in the Supporting Information for details. Magnetically induced current densities and related magnetic properties have been obtained using the CTOCD-DZ2 method with the SYSMOIC package<sup>[61]</sup> and adopting the B97-2 functional<sup>[62]</sup> in combination with the 6-311G(2d,2p) basis set.<sup>[63]</sup> For the implementation of the CTOCD methods at the DFT level see Refs. [64–67]. As it concerns the B97-2 functional, we have based our choice on the results by Flaig and coworkers,<sup>[68]</sup> who have shown, bench-marking hydrogen and carbon NMR chemical shifts, the good performance of the B97-2 functional for the calculation of accurate magnetic shielding constants. Since it is known that some functional tends to overestimate the paratropic ring-current strengths of strongly antiaromatic molecules, some authors recommend to employ also a functional with a larger percentage of HF exchange to avoid this kind of overestimation.<sup>[51,52]</sup> Functional with about 50% HF exchange yield ring current of about the same strength as obtained at the MP2 level.<sup>[53]</sup> Therefore, for the most paratropic species  $C_{70}H_{10}$  and  $C_{100}H_{10}$ , we have repeated the calculation adopting the M06-2X functional which has 54% HF exchange,<sup>[50]</sup> keeping same basis sets for geometry optimization and magnetic property calculation.

### Acknowledgements

Financial support from the MIUR (FARB 2017 and FABR 2018 to G.M. and R.Z.) and the US National Science Foundation (CHE-1149096 to L.T.S.) are gratefully acknowledged.

### Conflict of Interest

The authors declare no conflict of interest.

**Keywords:** aromaticity · density functional calculations · magnetic properties · nanotubes · cycloparaphenylene

- [1] L. T. Scott, E. A. Jackson, Q. Zhang, B. D. Steinberg, M. Bancu, B. Li, *J. Am. Chem. Soc.* **2012**, *134*, 107–110.
- [2] E. H. Fort, P. M. Donovan, L. T. Scott, *J. Am. Chem. Soc.* **2009**, *131*, 16006–16007.
- [3] E. H. Fort, L. T. Scott, *Angew. Chem. Int. Ed.* **2010**, *49*, 6626–6628; *Angew. Chem.* **2010**, *122*, 6776–6778.
- [4] E. H. Fort, L. T. Scott, *J. Mater. Chem.* **2011**, *21*, 1373–1381.
- [5] E. H. Fort, L. T. Scott, *Tetrahedron Lett.* **2011**, *52*, 2051–2053.

- [6] E. H. Fort, M. S. Jeffreys, L. T. Scott, *Chem. Commun.* **2012**, 48, 8102.
- [7] L. T. Scott, *Pure Appl. Chem.* **2017**, 89, 809–820.
- [8] A. Rochefort, D. R. Salahub, P. Avouris, *J. Phys. Chem. B* **1999**, 103, 641–646.
- [9] T. Sato, M. Tanaka, T. Yamabe, *Synth. Met.* **1999**, 103, 2525–2526.
- [10] T. Yamabe, M. Imade, M. Tanaka, T. Sato, *Synth. Met.* **2001**, 117, 61–65.
- [11] J. Li, Y. Zhang, M. Zhang, *Chem. Phys. Lett.* **2002**, 364, 338–344.
- [12] J. Cioslowski, N. Rao, D. Moncrieff, *J. Am. Chem. Soc.* **2002**, 124, 8485–8489.
- [13] Y. Matsuo, K. Tahara, E. Nakamura, *Org. Lett.* **2003**, 5, 3181–3184.
- [14] T. Yumura, S. Bandow, K. Yoshizawa, S. Iijima, *J. Phys. Chem. B* **2004**, 108, 11426–11434.
- [15] J. Zhao, P. B. Balbuena, *J. Phys. Chem. C* **2008**, 112, 13175–13180.
- [16] L. V. Liu, W. Q. Tian, Y. K. Chen, Y. A. Zhang, Y. A. Wang, *Nanoscale* **2010**, 2, 254–261.
- [17] F. J. Martín-Martínez, S. Melchor, J. A. Dobado, *Phys. Chem. Chem. Phys.* **2011**, 13, 12844.
- [18] P. W. Fowler, E. Steiner, R. W. A. Havenith, L. W. Jenneskens, *Magn. Reson. Chem.* **2004**, 42, S68–S78.
- [19] J. Juselius, D. Sundholm, J. Gauss, *J. Chem. Phys.* **2004**, 121, 3952–3963.
- [20] H. Fliegl, D. Sundholm, S. Taubert, J. Juselius, W. Klopper, *J. Phys. Chem. A* **2009**, 113, 8668–8676.
- [21] P. v R Schleyer, C. Maerker, A. Dransfeld, H. Jiao, N. J. R. v E Hommes, *J. Am. Chem. Soc.* **1996**, 118, 6317–6318.
- [22] Z. Chen, C. S. Wannere, C. Corminboeuf, R. Puchta, P. v R Schleyer, *Chem. Rev.* **2005**, 105, 3842–3888.
- [23] S. Pelloni, G. Monaco, P. Lazzeretti, R. Zanasi, *Phys. Chem. Chem. Phys.* **2011**, 13, 20666.
- [24] S. Pelloni, G. Monaco, R. Zanasi, P. Lazzeretti, *AlP Conf. Proc.* **2012**, 1456, 114.
- [25] R. Gershoni-Poranne, A. Stanger, *Chem. Eur. J.* **2014**, 20, 5673–5688.
- [26] I. Benkyi, O. Staszewska-Krajewska, D. T. Gryko, M. Jaszufski, A. Stanger, D. Sundholm, *J. Phys. Chem. A* **2020**, 124, 695–703.
- [27] A. Stanger, G. Monaco, R. Zanasi, *ChemPhysChem* **2020**, 21, 65–82.
- [28] E. Steiner, P. W. Fowler, L. W. Jenneskens, *Angew. Chem. Int. Ed.* **2001**, 40, 362–366; *Angew. Chem.* **2001**, 113, 375–379.
- [29] M. P. Johansson, J. Juselius, D. Sundholm, *Angew. Chem. Int. Ed.* **2005**, 44, 1843–1846; *Angew. Chem.* **2005**, 117, 1877–1880.
- [30] P. W. Fowler, A. Soncini, *Phys. Chem. Chem. Phys.* **2011**, 13, 20637.
- [31] G. Monaco, L. T. Scott, R. Zanasi, *J. Phys. Chem. A* **2008**, 112, 8136–8147.
- [32] P. Ren, A. Zheng, J. Xiao, X. Pan, X. Bao, *Chem. Sci.* **2015**, 6, 902–908.
- [33] G. Monaco, R. Zanasi, S. Pelloni, P. Lazzeretti, *J. Chem. Theory Comput.* **2010**, 6, 3343–3351.
- [34] G. Monaco, P. W. Fowler, M. Lillington, R. Zanasi, *Angew. Chem. Int. Ed.* **2007**, 46, 1889–1892; *Angew. Chem.* **2007**, 119, 1921–1924.
- [35] G. Monaco, R. Zanasi, *J. Phys. Chem. A* **2012**, 116, 9020–9026.
- [36] G. Monaco, R. Zanasi, *J. Phys. Chem. Lett.* **2017**, 8, 4673–4678.
- [37] E. Steiner, P. W. Fowler, *J. Phys. Chem. A* **2001**, 105, 9553–9562.
- [38] E. Steiner, P. W. Fowler, *Chem. Commun.* **2001**, 2220–2221.
- [39] J. Aihara, *Faraday Trans.* **1995**, 91, 237.
- [40] N. Nishina, M. Makino, J. Aihara, *J. Phys. Chem. A* **2016**.
- [41] R. Saito, G. Dresselhaus, M. S. Dresselhaus, *Physical properties of carbon nanotubes reprinted ed.*, Imperial College Press, London, **1999**, OCLC: 248714575.
- [42] J. L. Ormsby, B. T. King, *J. Org. Chem.* **2004**, 69, 4287–4291.
- [43] E. Clar, *The aromatic sextet*, J. Wiley, London, New York, **1972**.
- [44] M. Solà, *Front. Chem.* **2013**, 1, 22.
- [45] I. Gutman, S. Radenkovic, M. Antic, J. Djurdjevic, *J. Serb. Chem. Soc.* **2013**, 78, 1539–1546.
- [46] T. K. Dickens, R. B. Mallion, *J. Phys. Chem. A* **2018**, 122, 8865–8873.
- [47] B. A. Hess, L. J. Schaad, *J. Am. Chem. Soc.* **1971**, 93, 2413–2416.
- [48] A. Ciesielski, T. M. Krygowski, M. K. Cyrański, M. A. Dobrowolski, A. T. Balaban, *J. Chem. Inf. Model.* **2009**, 49, 369–376.
- [49] P. Lazzeretti, *Prog. Nucl. Magn. Reson. Spectrosc.* **2000**, 36, 1–88.
- [50] Y. Zhao, D. G. Truhlar, *Theor. Chem. Acc.* **2008**, 120, 215–241.
- [51] R. R. Valiev, H. Fliegl, D. Sundholm, *Chem. Commun.* **2017**, 53, 9866–9869.
- [52] R. R. Valiev, G. V. Baryshnikov, D. Sundholm, *Phys. Chem. Chem. Phys.* **2018**, 20, 30239–30246.
- [53] R. R. Valiev, I. Benkyi, Y. V. Konyshev, H. Fliegl, D. Sundholm, *J. Phys. Chem. A* **2018**, 122, 4756–4767.
- [54] D. W. Szczepanik, M. Solà, M. Andrzejak, B. Pawelek, J. Dominikowska, M. Kukulka, K. Dyduch, T. M. Krygowski, H. Szatyłowicz, *J. Comput. Chem.* **2017**, 38, 1640–1654.
- [55] M. Torrent-Sucarrat, S. Navarro, F. P. Cossío, J. M. Anglada, J. M. Luis, *J. Comput. Chem.* **2017**, 38, 2819–2828.
- [56] I. Casademont-Reig, T. Woller, J. Contreras-García, M. Alonso, M. Torrent-Sucarrat, E. Matito, *Phys. Chem. Chem. Phys.* **2018**, 20, 2787–2796.
- [57] I. Casademont-Reig, E. Ramos-Cordoba, M. Torrent-Sucarrat, E. Matito, *Molecules* **2020**, 25, 711.
- [58] M. J. Frisch, G. W. Trucks, H. B. Schlegel, G. E. Scuseria, M. A. Robb, J. R. Cheeseman, G. Scalmani, V. Barone, B. Mennucci, G. A. Petersson, H. Nakatsuji, M. Caricato, X. Li, H. P. Hratchian, A. F. Izmaylov, J. Bloino, G. Zheng, J. L. Sonnenberg, M. Hada, M. Ehara, K. Toyota, R. Fukuda, J. Hasegawa, M. Ishida, T. Nakajima, Y. Honda, O. Kitao, H. Nakai, T. Vreven, J. A. Montgomery Jr, J. E. Peralta, F. Ogliaro, M. Bearpark, J. J. Heyd, E. Brothers, K. N. Kudin, V. N. Staroverov, T. Keith, R. Kobayashi, J. Normand, K. Raghavachari, A. Rendell, J. C. Burant, S. S. Iyengar, J. Tomasi, M. Cossi, N. Rega, J. M. Millam, M. Klene, J. E. Knox, J. B. Cross, V. Bakken, C. Adamo, J. Jaramillo, R. Gomperts, R. E. Stratmann, O. Yazyev, A. J. Austin, R. Cammi, C. Pomelli, J. W. Ochterski, R. L. Martin, K. Morokuma, V. G. Zakrzewski, G. A. Voth, P. Salvador, J. J. Dannenberg, S. Dapprich, A. D. Daniels, O. Farkas, J. B. Foresman, J. V. Ortiz, J. Cioslowski, D. J. Fox, *Gaussian 09, Revision D.01*, Gaussian, Inc., Wallingford CT, **2013**.
- [59] A. D. Becke, *J. Chem. Phys.* **1993**, 98, 5648–5652.
- [60] W. J. Hehre, R. Ditchfield, J. A. Pople, *J. Chem. Phys.* **1972**, 56, 2257–2261.
- [61] G. Monaco, R. Zanasi, *SYSMOIC package*, University of Salerno, publication in progress, **2020**. The package can be downloaded upon request at <http://zanasi.chem.unisa.it>.
- [62] P. J. Wilson, T. J. Bradley, D. J. Tozer, *J. Chem. Phys.* **2001**, 115, 9233–9242.
- [63] M. J. Frisch, J. A. Pople, J. S. Binkley, *J. Chem. Phys.* **1984**, 80, 3265–3269.
- [64] J. R. Cheeseman, G. W. Trucks, T. A. Keith, M. J. Frisch, *J. Chem. Phys.* **1996**, 104, 5497–5509.
- [65] R. W. A. Havenith, P. W. Fowler, *Chem. Phys. Lett.* **2007**, 449, 347–353.
- [66] A. Soncini, A. M. Teale, T. Helgaker, F. De Proft, D. J. Tozer, *J. Chem. Phys.* **2008**, 129, 074101.
- [67] R. W. A. Havenith, A. J. H. M. Meijer, B. J. Irving, P. W. Fowler, *Mol. Phys.* **2009**, 107, 2591–2600.
- [68] D. Flaig, M. Maurer, M. Hanni, K. Braunger, L. Kick, M. Thubauville, C. Ochsenfeld, *J. Chem. Theory Comput.* **2014**, 10, 572–578.

Manuscript received: April 2, 2020

Revised manuscript received: May 6, 2020